CHARACTERISTICS OF SEDIMENT TRANSPORT IN SWASH ZONE DUE TO SATURATED-UNSATURATED SLOPED BEACH

Masashi Ochi[1], Makoto Miyatake[2] and Katsutoshi Kimura[3]

The influence of saturated-unsaturated sloped beach on sediment transport in swash zone was investigated experimentally and numerically. The movement of fluorescent sand on seabed and the orbit of fluorescent paint injected into the sandy beach were measured in bore wave experiments. As the result, the uplift seepage flow leads to the activation of sediment transport in the direction of run-up and backwash under the saturated slope. The numerical modeling simulated the interacting swash wave motion and saturated-unsaturated coastal seepage flow. The tractive force under the influence of seepage flow was quantified through a permeable Shields parameter. The results of prediction are in good qualitative agreement with those of experiments.

Keywords: swash sediment transport; saturated-unsaturated slope; wave-driven seepage flow

1. Introduction

Roads, railways and residential areas along the coastline are damaged due to storm-induced erosion in Japan. Infiltration and exfiltration flux across the beach face is one of the factors that need to consider for sediment mobility in swash zone. The significant knowledge to this problem has been gained over many years from previous studies. For example, Turner and Masselink (1998) have quantified sediment transport under the influence of wave-induced seepage flow through a permeable Shields parameter concerned with both the effective weight of sediment particles and the swash boundary layer thickness. A numerical approach due to a Boussinesq model coupled with a porous flow model to estimate the sediment transport in swash zone has been presented by Karambas (2002). However, with most of these researches, the seepage flow simply has been considered as 1-dimensional vertical saturated theory. The characteristics of wave-driven 2-dimensional saturated-unsaturated seepage flow have not been well understood. In particular, the effect of saturated-unsaturated seepage flow on sediment transport may have an important implication for the shore erosion process under storm conditions.

In this study, the measurements of swash motion are not easy due to influence of turbulence and to interference with previous waves. Therefore using a bore wave, the experiments that simplified the phenomenon of swash motion are conducted to clarify the characteristics of sediment transport in swash zone due to the saturated-unsaturated sloped beach. A numerical approach for coupling run-up waves with porous flow in a coastal aquifer and estimation of the tractive force under the influence of seepage flow are presented. The effects of saturated-unsaturated seepage flow on sediment transport in swash zone are investigated through the present model calculations.

2. Sediment Transport and Seepage Flow Visualization Experiments in Swash Zone

2.1 Sediment Transport Experiment using Fluorescent Sand

The experiments were performed in a 0.4 m wide, 0.4 m deep and 10.2 m long wave channel as shown in Figure1. A sloping beach constructed at right side of the channel was 2.5 m long and 0.24 m height with a gradient of 1/10. The seabed comprises of silica sand, with a median grain size of 0.1 mm, a specific gravity of 2.67 and a hydraulic conductivity of 0.0144 cm/s. The initial phreatic surface and saturation in the sandy beach were controlled by the backshore water level *H'* varied from 5 cm to 15 cm (such as the table in Figure 1). A single broken bore was generated by opening the water gate at the end of the channel as an incident wave. The water level behind the gate was 40 cm and all experiments worked with a still water level of 5 cm. The fluorescent sand (green color) layer with 1cm deep and 10cm long was laid on beach slope so as to be center position at 50 cm onshore from still water shoreline. The movement of fluorescent sand due to run-up and backwash wave was recorded by a digital video camera under the black light shining. The tracking images of RGB color were extracted from the mpeg-formatted movie with time sampling of 0.033s. All obtained images separated into

[1]Department of Civil Engineering and Architecture, Muroran Institute of Technology, 27-1 Mizumoto-cho, Muroran, 050-0071, Japan
[2]Department of Civil Engineering, Hakodate National College of Technology, 14-1 Tokura-cho, Hakodate, 042-8501, Japan
[3]Department of Civil Engineering and Architecture, Muroran Institute of Technology, 27-1 Mizumoto-cho, Muroran, 050-0071, Japan

images of fluorescent sand(green color) components and converted to gray scale. Figure 2 shows the relationship between gray scale brightness of tracking image and sediment transport concentration of fluorescent sand in several condition. In order to exchange from this gray scale brightness to sediment transport concentration, we make a solid curve fitted with an exponential function.

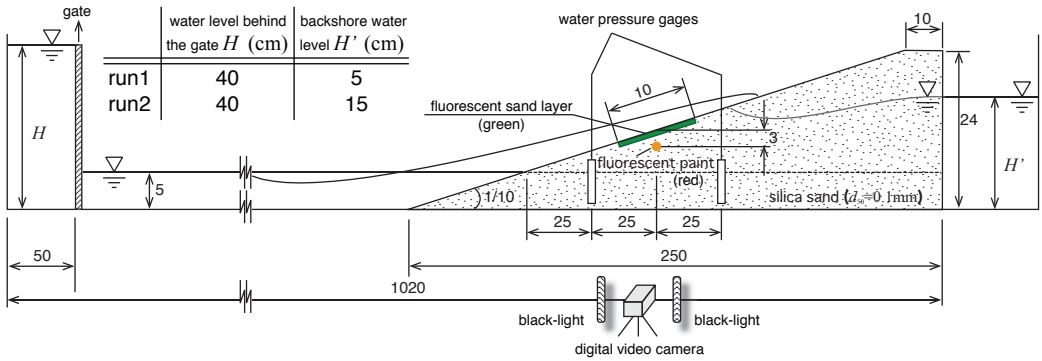

Figure 1. Experimental Setup (Unit : cm)

2.2 Seepage Flow Experiment using Fluorescent Paint

The seepage flow experiment were carried out as same as the condition of sediment transport experiment. The number of bore waves with the gate water level 40cm was fixed to five times with an interval of 180 s. The orbits of fluorescent paint injected into the sandy beach model were recorded by a digital video camera as similar to the sediment transport experiment. Each measurement of sub-surface pore pressure below the bed was positioned at a distance of 25 cm from the fluorescent injection point. The water surface elevation of run-up waves was also measured by a digital video camera.

The relationship between gray scale brightness of tracking images and volumetric concentration of the fluorescent paint were investigated through photographic observations in several conditions. All tracking images given from mpeg-formatted movies were converted from RGB colors to gray scale. Figure 3 shows the result of measurements. The gray scale brightness B reaches an upper limit while the volumetric concentration is in more than 70%. Thereby the fluorescent paint of volumetric concentration in the range from 5% to 40% was used for all experiments. The solid line in this figure was fitted with an exponential function in order to exchange from the gray scale brightness to the volumetric concentration. From this, we can obtain the volumetric concentration in tracking images by using the gray scale transformation curve.

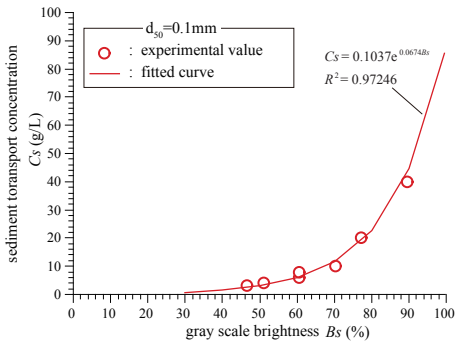

Figure 2. Gray Scale Transformation Curve (Fluorescent Sand)

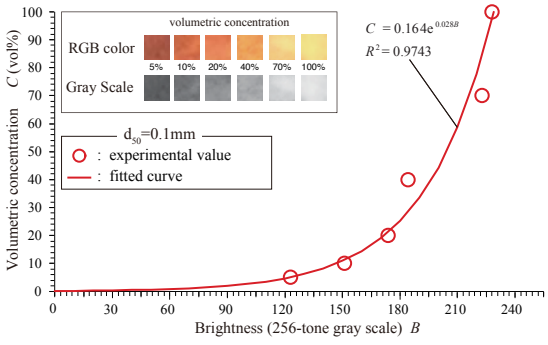

Figure 3. Gray Scale Transformation Curve (Fluorescent Paint)

2.3 Inversed Estimation of Wave-Driven Seepage Flow

Assuming the volumetric concentration obtained from tracking images of fluorescent paint is transported by wave-driven seepage flow, the governing equation related to the advection diffusion of fluorescent paint can be described as follows:

$$\frac{\partial C}{\partial t}+u'\frac{\partial C}{\partial x}+w'\frac{\partial C}{\partial z}=\frac{\partial}{\partial x}\left\{(\alpha_L\frac{u'}{V}+D_M)\frac{\partial C}{\partial x}\right\}+\frac{\partial}{\partial z}\left\{(\alpha_T\frac{w'}{V}+D_M)\frac{\partial C}{\partial z}\right\} \quad (1)$$

where C is the volumetric concentration, u' and w' are the actual velocities given from dividing the seepage velocities u and w by the void ratio λ, V is its synthetic velocity, α_L, α_T, D_M are the coefficients related to water molecular diffusivity.

This above equation is generally used to estimate the concentration by giving the actual velocity. However here work analyzed the wave-driven seepage flow velocity as an inversed problem using the time-space variation of volumetric concentration in tracking images. By setting the actual velocities u' and w' as the estimation parameters $\mathbf{P}$, the objective function can be written as

$$E(\mathbf{P})=\sum_{J=1}^{m}\left\{C(J,\mathbf{P})-\hat{C}(J)\right\}^2=\sum_{J=1}^{m}s_J^2 \quad (2)$$

where $C(J,\mathbf{P})$ is the volumetric concentration computed from equation (1), $\hat{C}(J)$ is the volumetric concentration obtained from photographic observations, s_J is the output error, J is the pixel number and m is the number of total pixels of a tracking image.

To minimize the objective function by adding the correction factors $\mathbf{e}$ to the estimation parameters $\mathbf{P}$, the first derivative of the objective function sets to zero as follows:

$$\frac{\partial}{\partial \mathbf{P}}E(\mathbf{P}+\mathbf{e})=0 \quad (3)$$

Applying a Taylor series expansion to equation (3), a first order approximation can be given as

$$\frac{\partial}{\partial \mathbf{P}}E(\mathbf{P}+\mathbf{e})=2\left(\mathbf{A}^t\cdot\mathbf{s}+\mathbf{A}^t\cdot\mathbf{A}\cdot\mathbf{e}\right)=0 \quad (4)$$

where $\mathbf{A}$ is the matrix of l rows and m columns with $A_{J,l}=\partial s_J/\partial p_l$ components, l is the number of estimation parameters. From this, the correction factors $\mathbf{e}$ can be obtained as

$$\mathbf{e}=\left(\mathbf{A}^t\cdot\mathbf{A}\right)^{-1}\cdot\mathbf{A}^t\cdot\mathbf{s} \quad (5)$$

The correction factors $\mathbf{e}$ are computed using equation (5). The estimation parameters $\mathbf{P}$ modified by the correction factors $\mathbf{e}$ are determined by iterative calculations so as to satisfy the relative error as follows:

$$\sum_{J=1}^{m}\frac{C(J,\mathbf{P})-\hat{C}(J)}{C(J,\mathbf{P})}<0.0001 \quad (6)$$

Finally, the seepage velocities u and w can be given by multiplying the actual velocities u' and w' to the void ratio.

3. Sediment Transport and Seepage Flow Characteristics of Saturated-Unsaturated Slope

3.1 Characteristics of Sediment Transport due to Saturated-Unsaturated Slope

Figure 4 and Figure 5 shows the brightness concentration distribution of fluorescent sand under unsaturated (H' = 5 cm) and saturated (H' = 15 cm) slope. The upper and lower parts of these figures indicate the snapshots in which the sediment transport is the largest during the run-up and backwash phase respectively. In comparison with the brightness concentration of the run-up and backwash phase, this brightness concentration at backwash phase becomes higher regardless of whether the beach slope is saturated or unsaturated. The increment of sediment transport at backwash seems to be caused by lifting the bed sands due to backwash wave in addition to the residual suspended sediment components at run-up phase.

In the run-up phase of a bore wave, the brightness concentration becomes higher according to the run-up wave arrives. Especially, the highest concentration around seabed can be seen clearly in both

slopes. This brightness concentration of saturated slopes are higher than those of unsaturated slope. This means that the even more lifted sands are transported to onshore direction with the run-up wave in case of saturated slope. Meanwhile in the backwash phase, the brightness concentration in case of saturated slope becomes also higher as similar to run-up phase in comparison with unsaturated slope. In the case of saturated slope, it leads to the activation of the sediment transport in the direction of onshore and offshore at both the run-up and backwash.

Figure 6 indicates the time series of the quantity of fluorescent sand unit per width obtained from gray scale brightness of tracking images at the unsaturated and saturated slope, respectively. When the seabed is saturated, the sediment transport in the direction of run-up and backwash becomes constantly larger compared with unsaturated slope. Especially the significant change in direction of backwash can be seen. The effects of saturated-unsaturated slope make clearly at backwash phase.

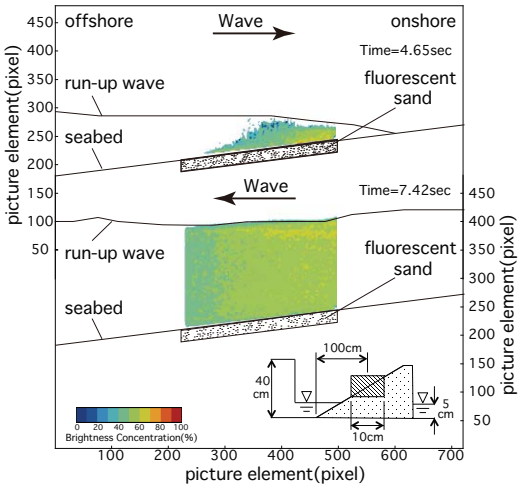

Figure 4. Unsaturated slope (H' = 5cm)

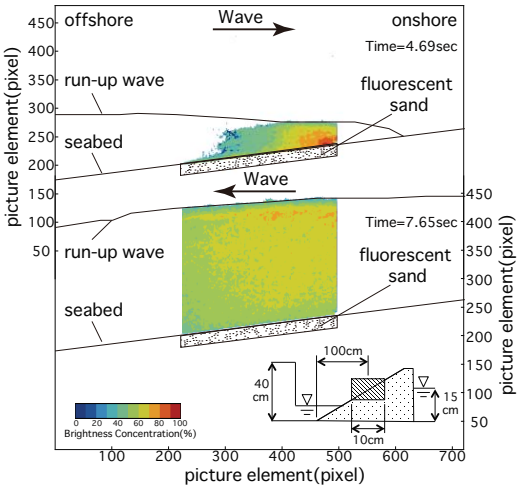

Figure 5. Saturated slope (H' = 15cm)

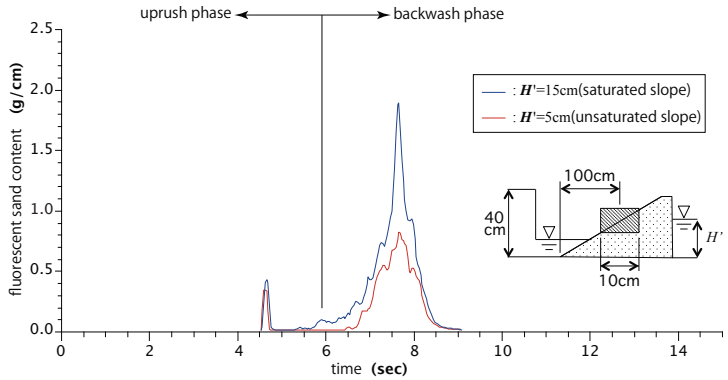

Figure 6. Time series of fluorescent sand transport per unit width

3.2 Characteristics of Wave-Driven Seepage Flow

Figure 7(a) shows the volumetric concentration of fluorescent paint and estimated seepage velocity at the backshore water level H'=15 cm. When the seabed is saturated, the seepage vectors varied from seaward to upward can be seen on backwash. The mean velocity of seepage is approximately 10^{-3} cm/s. The order of velocity is nearly equal to Darcian velocity determined from the difference of pore pressure between two measuring points. Thereby, wave-driven seepage flow is activated by horizontal pore pressure gradients. These patterns of seepage flow may be one of significant contributing factors for increasing of sediment transport. Figure 7(b) indicates the case of H'=5 cm. In case of the unsaturated seabed, the seaward and upward seepage flow become weaker

compared with the saturated case. From these, the wave-driven unsaturated-saturated seepage flow may have an important implication for the quantity of sediment transport in swash zone.

Figure 8 gives the results of water surface and sub-surface elevation measurements at a distance of 25 cm towards offshore and onshore from the fluorescent injection point. Figure 8(a) indicates the case of H'=15 cm. At offshore side, the rising of phreatic surface is almost contemporaneous with the increasing of water surface elevation of wave run-up. Conversely, the rising of phreatic surface at onshore side tends to delay compared with wave run-up. The steep gradients of phreatic surface on backwash seems to accelerate the seaward and upward seepage flow in the saturated condition. On the other hand, in Figure 8(b), the onshore side of phreatic surface in the case of H'=5 cm remains nearly constant after the rising. It means that water infiltration is stored into backshore and the seaward and upward seepage flow is weakened in the unsaturated condition.

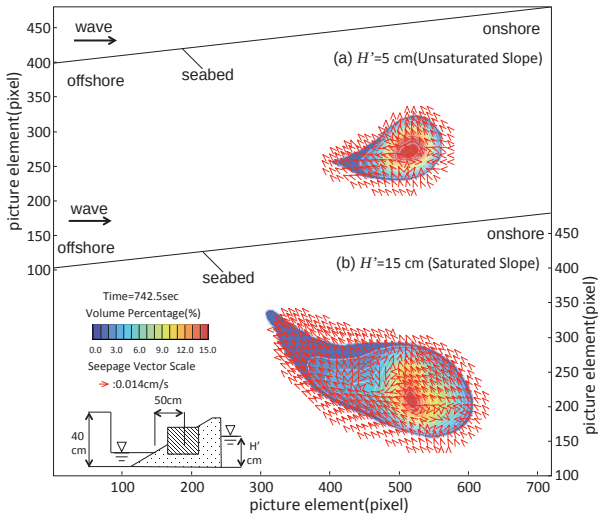

Figure 7 Distributions of volumetric concentration and estimated seepage flow vectors on backwash

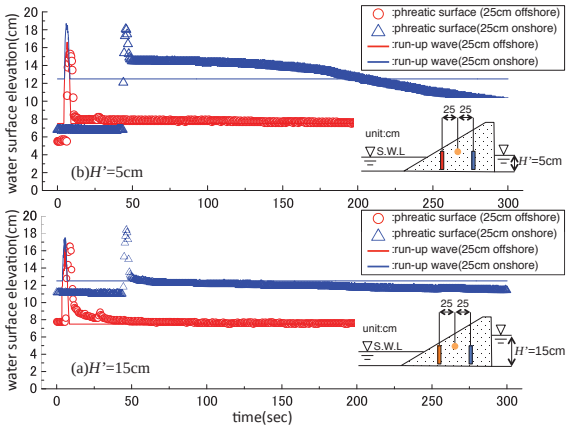

Figure 8 Time Series of Water Surface of Run-up and Sub-surface Elevation

4. Dimensionless Tractive force Model of Saturated-Unsaturated Slope

4.1 Governing Equations for Seepage Flow

The porous flow in a coastal aquifer, as governed by the saturated-unsaturated seepage flow equations (Bear, 1979), is considered in this model. Hydraulic head-based equations can be written as

$$(u,w) = -K(\psi)\left(\frac{\partial \psi}{\partial x}, \frac{\partial \psi}{\partial z} + 1\right) \tag{7}$$

$$\{S_w S_s + C(\psi)\}\frac{\partial \psi}{\partial t} = \frac{\partial}{\partial x}\left\{K(\psi)\frac{\partial \psi}{\partial x}\right\} + \frac{\partial}{\partial z}\left\{K(\psi)(\frac{\partial \psi}{\partial z}+1)\right\} \quad (8)$$

where u and w are the seepage velocities, $K(\psi)$ is the permeability, ψ is the pressure head in the positive value and in the case of negative indicates the capillary head, S_s is the specific storage coefficient, S_w is the effective saturation.

As the relationship between capillary head ψ and water content θ required for these model calculations, we use the water retention curves shown on Figure 9 obtained by laboratory tests. The solid and dot lines in the figure are fitted with a Van-Genuchten (1980) formula, which is defined as

$$\theta = \theta_s + (\theta_s - \theta_r)\left\{\frac{1}{1+(a|\psi|)^n}\right\}^m \quad (9)$$

where θ_s is the porosity, θ_r is the residual water content, a, m and n are the constants.

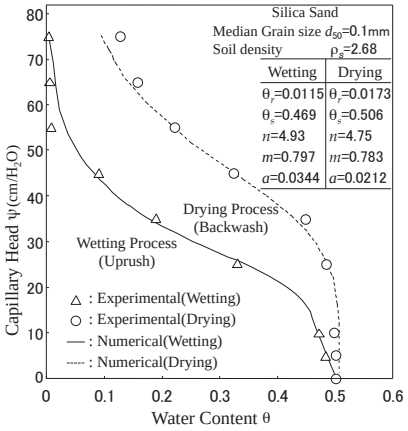

Figure 9. Water Retention Curve

4.2 Governing Equations for Swash motion

Navier-Stokes equations are used to describe the wave transformation on a beach slope as follows:

$$\frac{\partial U}{\partial x} + \frac{\partial W}{\partial z} = 0 \quad (10)$$

$$\frac{\partial U}{\partial t} + \frac{\partial U^2}{\partial x} + \frac{\partial UW}{\partial z} = -\frac{1}{\rho}\frac{\partial p}{\partial x} + \nu\left(\frac{\partial^2 U}{\partial x^2} + \frac{\partial^2 U}{\partial z^2}\right) \quad (11)$$

$$\frac{\partial W}{\partial t} + \frac{\partial UW}{\partial x} + \frac{\partial W^2}{\partial z} = g - \frac{1}{\rho}\frac{\partial p}{\partial z} + \nu\left(\frac{\partial^2 W}{\partial x^2} + \frac{\partial^2 W}{\partial z^2}\right) \quad (12)$$

$$\frac{\partial \zeta}{\partial t} + \frac{\partial}{\partial x}\int_{-h}^{\zeta} U\,dz = 0 \quad (13)$$

where U and W are the water particle velocities, p is the water pressure, ν is the kinematic viscosity coefficient, g is the gravity acceleration, ζ is the water surface elevation. The computation of run-up and down wave fronts is carried out as the moving boundary condition (Shibayama et al., 2002).

4.3 Computation Method

Equations (7) ~ (13) are solved using the finite difference method applied the natural coordinates. Both the wave transformation and porous flow models are coupled through hydraulic head on the seabed boundary. The other boundary conditions are same as those of the experiments. The computations are performed by two different groundwater conditions as similar to the experiments.

4.4 Dimensionless Tractive Force Model of Permeable Slope

We examine the sediment transport under the influence of wave-induced seepage flow by using non-dimensional tractive force. Although the observed sediment transport in experiment has contained the components of suspended load from the photographic analysis, the effect of seepage flow on suspended load has not made clear yet from the results of this experiments. As a preliminary study, the external force of sediment transport in swash zone is evaluated by the tractive force incorporated the seepage effects approximately.

As dimensionless tractive force under the influence of the seepage flow, we used permeable Shields parameter proposed by Tuner and Masselink in 1998. This model is concerned with both the effective weight of sediment and the swash boundary layer thickness. This modified shields parameter has estimated using the run-up wave bottom velocity and the infiltration-exfiltration velocity obtained from

numerical simulations. Using the results of numerical solution, the dimensionless tractive force Θ_w is calculated by following equation:

$$\Theta_w = \frac{\tau_w}{W_w} = \frac{\tau_0 \left(\frac{\Phi}{e^{\Phi} - 1} \right)}{\rho_w g d \left(s - 1 - \beta \frac{w_s}{K(\psi)} \right)} \tag{14}$$

$$\Phi = \frac{c}{f} \frac{w_s}{|u_s|} \tag{15}$$

where f is the coefficient of bottom friction, s is the specific gravity of sediment grain, d is the median grain size of sediment, τ_0 ($=0.125\rho f U^2$) and τ_w indicate impermeable and permeable bottom tractive force respectively, u_s is the bottom velocity of run-up wave as the positive value to onshore direction, w_s is the infiltration velocity in the positive value and in the case of negative indicates the exfiltration velocity, $K(\psi)$ is the permeability, W_w is the effective weight of sediment grain, c defines a constant, and f is a friction factor for the case of no through-bed flow. The constant c relates to the nonlinear relation between shear stress and infiltration (Conley and Inman, 1994). The theoretical value for steady flow is adopted here, c =2.0, according to Turner and Masselink (1998) and Butt et al. (2001). The friction factor f is estimated using the formula based on Butt et al. (2001) and Karambas (2003).

5. Results of Numerical Analysis

Figure 10 gives the comparison between the numerical results and the experimental data. Time series of water surface and sub-surface elevation at two measuring points are plotted. The numerical results are agreed well with the experimental ones. We have confirmed that the other cases also reproduced the experimental results accurately.

Figure 11 shows the computed seepage vectors distribution at backwash for backshore water level H' at 5 cm and 15 cm, respectively. The seaward and upward groundwater flow can be seen as similar to the experimental results. The flux exfiltrated from the seepage face due to discontinuity of water surface of run-up wave and phreatic surface becomes larger according as the phreatic surface rises. This uplift seepage seems to lead to the unstable condition of the beach face on backwash.

Figure 12(a), (b), (c) and (d) shows the time series of run-up wave bottom velocity u_s and infiltration-exfiltration velocity w_s, bottom tractive force τ, sand grain effective weight W and dimensionless tractive force Θ respectively. From comparing permeable slope with impermeable ones through the bottom tractive force and the sand particle effective weight, we can see that the bottom tractive force of permeable slope τ_w defined as numerator of Tuner and Masselink model becomes similar to τ_0 of impermeable slope, which is not influenced by infiltration-exfiltration process. The effect of infiltration-exfiltration on swash boundary layer thickness is not confirmed under this experiment condition. On the other hand, increase or decrease of effective weight in cases of permeable slope W_w defined as denominator of Tuner and Masselink model can be seen clearly in comparison with W_0 of impermeable slope. In case of permeable slope, the effective weight of sand particle is increased by the infiltration due to run-up wave and decreased by the exfiltration due to backwash wave. The infiltration-exfiltration process significantly affects the effective weight of sand particle in concerning with permeable slope. As the result, in comparing with impermeable slope, the dimensionless tractive force of permeable slope Θ_w becomes smaller in run-up phase and larger in backwash phase regardless of the saturated-unsaturated slope.

Comparing the dimensionless tractive force of permeable slope Θ_w between saturated and unsaturated, in case of saturated condition, it becomes larger toward both offshore and onshore, which is mainly caused by change of the effective weight of sediment grains due to infiltration and exfiltration process. Although this dimensionless tractive force computed by the present model may not be directly comparable with the sediment transport obtained from experiments, the results of prediction are in good qualitative agreement with those of experiments.

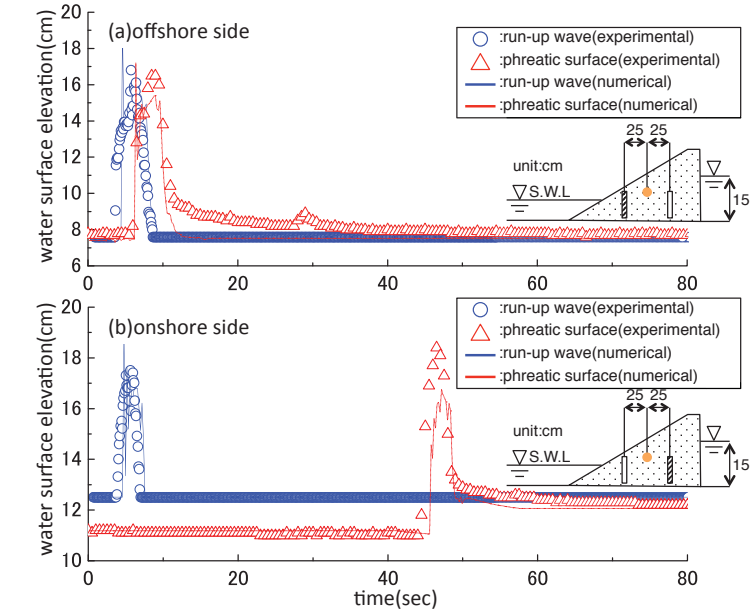

Figure 10 Comparison of simulated and measured water surface and sub-surface elevation

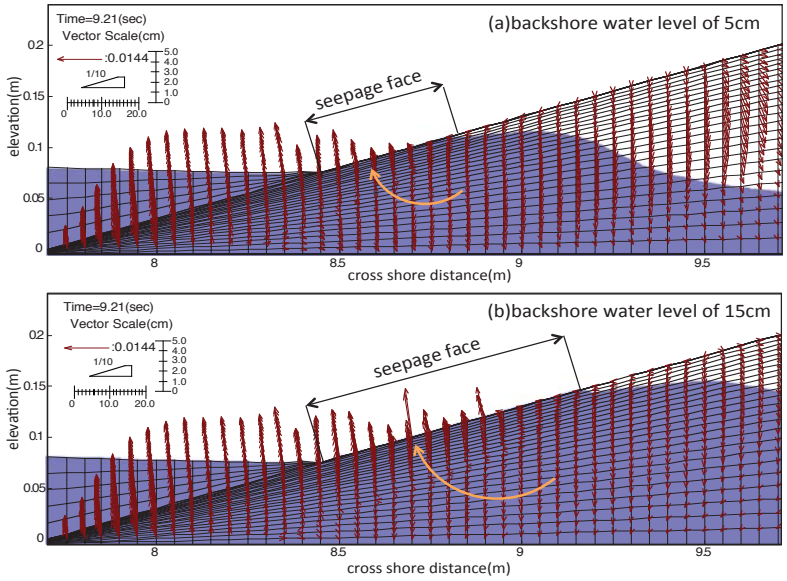

Figure 11 Wave-driven seepage flow distribution on backwash

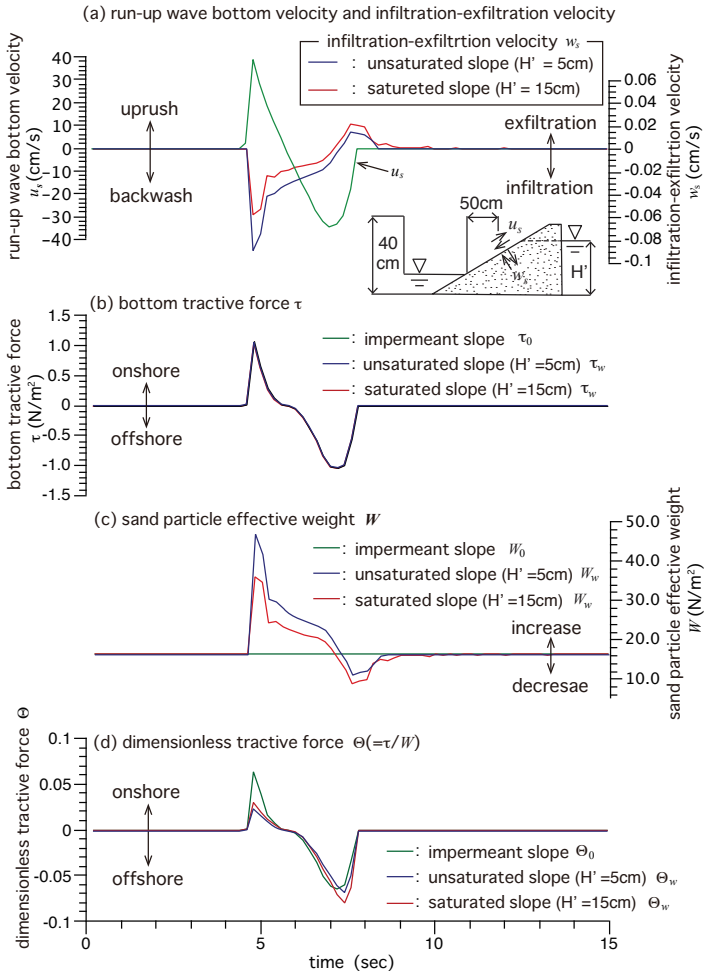

Figure 12 Time Series of Dumensionless Tractive Force Computed by the Present Model

6. Conclusions

1. In case of saturated slope, the sediment transport in the direction of run-up and backwash becomes constantly larger compared with unsaturated slope.
2. The uplift seepage force due to exfiltration leads to the activation of sediment transport in the direction of backwash under the saturated slope.
3. In case of saturated condition, it becomes larger toward both offshore and onshore, which is mainly caused by change of the effective weight of sediment grains due to infiltration and exfiltration process.

REFERENCES

Tuner, I. L. and Masselink, G., 1998. Swash infiltration-exfiltration and sediment transport, *J. Geophys. Res.*, 103, pp. 30813-30824.

Karambas, Th.V., Koutitas, C., 2002. Surf and swash zone morphology evolution induced by nonlinear waves. *Journal of Waterway, Port, Coastal, and Ocean Engineering* 128 (3), pp. 102–113.

Bear, J., 1979. Hydraulic of groundwater, *McGraw-Hill*, pp.190-224.

Van-Genuchten, M. T., 1980. A closed-form equation for predicting the hydraulic conductivity of unsaturated soils, *Soil Science Society of America Journal*, 44, pp. 892-898.

Sibayama, T. and Duy, T. N., 2002. A Simulation of Swash Oscillations by Two-Dimensional Vertical Breaking Wave Model, *Proceedings of Coastal Engineering, JSCE*, 49, pp.451-455.

Butt, T., Russell, P., Turner, I. 2001. The influence of swash infiltration- exfiltration on beach face sediment transport: onshore or offshore?, *Coastal Engineering*, 42, No. 1, pp.35-52.

Conley, D.C., Inman, D., 1994. Ventilated oscillatory boundary layers, *Journal of Fluid Mechanics*, 273, pp.261–284.

Karambas, T. V., 2003. Modelling of infixtration-exfiltration effects of cross-shore sediment transport in the swash zone, *Coastal Engineering*, 45, No. 1, pp. 63-82.